Nano Approach Investigation of the Conduction Mechanism in Polyaniline Nanofibers

Yen-Fu Lin,[†] Chien-Hsiang Chen,[†] Wen-Jia Xie,[†] Sheng-Hsiung Yang,[‡,||] Chain-Shu Hsu,[‡] Minn-Tsong Lin,[§,⊥] and Wen-Bin Jian[†,*]

[†]Department of Electrophysics, and [‡]Department of Applied Chemistry, National Chiao Tung University, Hsinchu 30010, Taiwan, [§]Department of Physics, National Taiwan University, Taipei 10617, Taiwan, and [⊥]Institute of Atomic and Molecular Sciences, Academia Sinica, Taipei 10617, Taiwan. [||] Present address: Institute of Lighting and Energy Photonics, National Chiao Tung University, Gueiren Township, Tainan, 711, Taiwan.

Polyaniline has been known for more than 150 years.[1] This material and its counterparts of conducting polymers have aroused considerable interests since the 1980s,[2] and during that time, most reports focused on chemical synthesis, oxidation–reduction reaction, chemical structures, lattice phases,[3] and the conduction mechanism in polymers.[4] Most recently, polyaniline has caught the eyes of scientists again because new synthesis processes, such as interfacial polymerization, have been developed to produce this material with more nanofibrillar morphology in contrast to granular and agglomerated polyaniline bulk, synthesized with conventional chemical oxidation or electrochemical polymerization in aqueous acids.[2,5] The growing attention on polyaniline is due not only to manifold applications, such as gas sensors,[6] actuators,[7] field-effect transistors,[8] memory devices,[9] and electrochemical capacitors,[10] but also to exploration of the mechanism of nanofiber formation[5,11] in application to other conducting polymers. Polyaniline consists of three oxidation states including leucoemeraldine, emeraldine, and pernigraniline base form.[2] The emeraldine base form of polyaniline can be doped (protonated) to form emeraldine salt by an acid such as HCl, and conversely, the emeraldine salt form can be dedoped back by a base.[2] The protonation process causes a conductivity variation from $\sim 10^{-10}$ to $10\ \Omega^{-1}\ cm^{-1}$.[12]

Research into the conduction mechanism of polyaniline began right after its rediscovery in the 1980s. Zuo et al.[12] studied the temperature-dependent thermopower, the temperature and electric field (with an applied voltage up to 100 V) dependence of

ABSTRACT A nanotechnological approach is applied to measurements of the electric field dependence of resistance under a high electric field while in low voltage. With this technique, the conduction mechanism on a mesoscopic scale is explored in a single, nonagglomerated nanofiber. Polyaniline nanofibers are prepared by vigorous mixing of aniline and oxidation agent ammonium persulfate in acid solution. They exhibit a uniform nanoscale morphology rather than agglomeration as that produced via conventional chemical oxidation. The as-synthesized polyaniline nanofibers are doped (dedoped) with a HCl acid (NH_3 base), and their temperature behaviors of resistances follow an exponential function with an exponent of $T^{-1/2}$. To measure the conduction mechanism in a single nanofiber, the dielectrophoresis technique is implemented to position nanofibers on top of two electrodes with a nanogap of 100–600 nm, patterned by electron-beam lithography. After the devices are irradiated by electron beam to reduce contact resistances, their temperature behaviors and electric field dependences are unveiled. The experimental results agree well with the theoretical model of charging energy limited tunneling. Other theoretical models such as Efros-Shklovskii and Mott's one-dimensional hopping conduction are excluded after comparisons and arguments. Through fitting, the size of the conductive grain, separation distance between two grains, and charging energy per grain in a single polyaniline nanofiber are estimated to be about 4.9 nm, 2.8 nm, and 78 meV, respectively. The nanotechnological approach, where the nanogap and the dielectrophoresis technique are used for single nanofiber device fabrication, is applied for determination of mesoscopic charge transport in a polyaniline conducting polymer.

KEYWORDS: conducting polymer · one-dimensional nanostructures · polyaniline · hopping conduction · nanofiber

polyaniline film conductivity, and protonation level. They argued that the theory of charging energy limited tunneling (CELT) proposed by Sheng et al.[14] gives an adequate description of the conduction mechanism. They believed that the protonated polyaniline forms metallic regions, modeled as a sphere of metal grain, and the unprotonated polyaniline forms an insulating region which results in a separation between conductive grains. According to Sheng's theory, they estimated the most probable distance of a conductive grain with a grain separation to be 20–27 nm. Wang et al.[15]

carried out similar experiments and an additional measurement of the temperature-dependent dielectric constant. In contrast, they concluded that polyaniline is a one-dimensional (1D) disordered conductor, complying with Mott's variable range hopping (VRH) theory, while an interchain coupling makes these 1D intrachain localized states constitute three-dimensional (3D) delocalized states. Li et al.[16] proposed a granular-rod model to explain the temperature dependence of the conductivity, the doping dependence, the thermoelectric power, and the Pauli susceptibility of polyaniline. Their model was comparable with the 3D VRH theory with an additional assumption of linear temperature-dependent density of states near the Fermi level. Pelstar et al.[17] gave a similar model and suggested that the conducting, crystalline regions are surrounded by an insulating, amorphous region. They used their model to estimate the diameter of metallic regions and the barrier width (separation) to be about 8 and 1.6 nm, respectively. Moreover, they implied that the model can also be compatible with Sheng's CELT model. Zuppiroli et al.[18] reexamined the implementation of the CELT model to hopping in disordered conducting polymers and used it to evaluate the diameter of conducting grains and the separation. They additionally provided a detailed description of protonation-induced interchain coupling, thus they took polaronic clusters as conducting grains. In the following years, several other experiments each supported different models including 3D VRH,[19] 1D VRH with interchain coupling,[20] crystalline regions connected through amorphous regions,[20] Efros-Schklovskii (ES) hopping conduction,[21] CELT (granular metallic) model,[22,23] and the localization interaction model.[24] In those reports, it is argued that the charge transport should be clarified on a *mesoscopic* scale and the *true* mechanism of electron transport in polyaniline is still under debate.

Recently, a new electrospinning technique has been developed to produce polymeric nanofibers with a submicrometer diameter.[25−27] Moreover, electrical property measurements on polymer nanofibers and nanotubes were carried out,[28,29] and it was commented that the *internanotubular contacts* should play a vital role on the temperature-dependent conductivity of polyaniline films.[28] Until now, there are still a lot of debates and controversies on the conduction mechanism in polyaniline. The summary of a survey of literature indicates that the conductivity problem resides in mesoscopic physics and its nanofibrillar nature. Particularly, the field dependence of conductivity shall be measured and studied in a more careful manner to prevent a high applied voltage, leading to high energy damaging effects. In this article, we will briefly describe conduction mechanisms in polyaniline from microscopic, mesoscopic, and macroscopic viewpoints. To explore the conduction mechanism on a mesoscopic
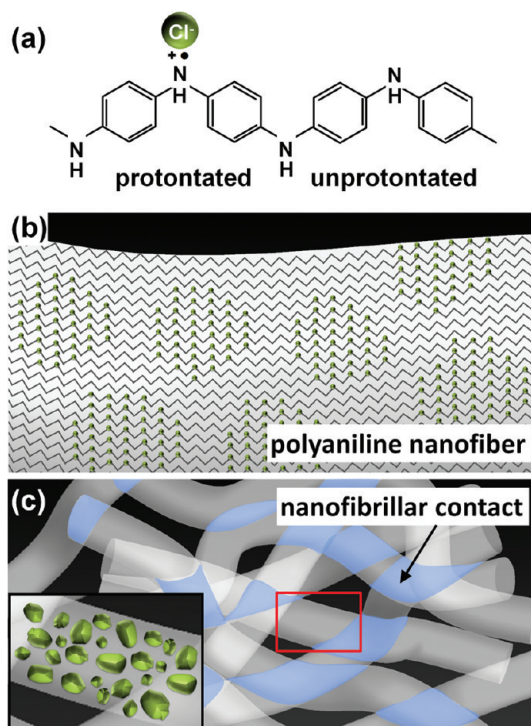

Figure 1. (a) Sketch of a chemical structure of unprotonated and HCl-protonated polyaniline units. (b) Partially protonated polyaniline nanofiber. The solid zig-zagged lines and the green dots represent polyaniline chains and Cl atoms, respectively. The grain feature of protonated regimes is implicated, as well. (c) Scheme of entangled polyaniline nanofibers. The internanotubular contacts are marked in blue on the graph. The inset indicates a close view of the red rectangle area. The 3D green regimes in the inset illustrate the protonated grain structures in a single polyaniline nanofiber.

scale, we implement a dielectrophoresis technique, which has not been applied to a study of the conduction mechanism in polyaniline yet, to examine temperature and electrical field dependences of a single polyaniline nanofiber with a diameter of about 50 nm and a length of 100−600 nm. According to our experimental results, we argue that Sheng's CELT model gives the best description of electron transport in polyaniline on a mesoscopic scale.

RESULTS AND DISCUSSION

We start to describe and discuss the issue of electron transport in polyaniline before stepping into experimental results. Figure 1a shows a chemical structure of protonated (emeraldine salt on the left) and unprotonated (emeraldine base to the right) polyaniline units. In a first step and starting from a microscopic viewpoint, it is disclosed[30] that an unprotonated polyaniline chain reveals a semiconductor-like band structure with a band gap energy of ∼4 eV. This seems to be in connection with the Coulomb energy between two non-overlapping electrons sitting at a distance of the size of the monomer.[18] Since the size of the monomer a is ∼0.35 nm, the unscreened Coulomb potential
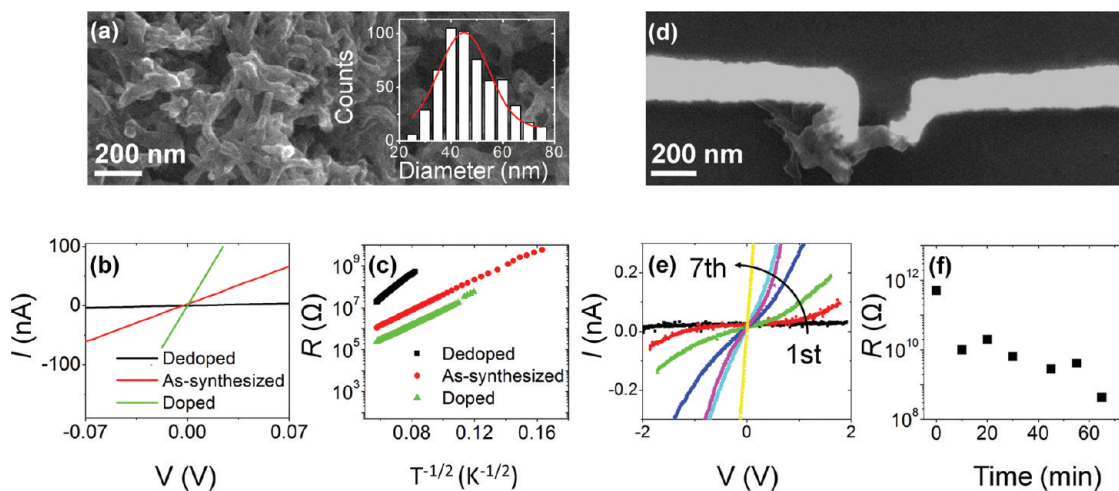
Figure 2. (a) SEM image of as-synthesized polyaniline nanofibers. The inset shows a size distribution and a red line of fitting to the Gaussian function. The average diameter and the standard deviation of nanofibers are evaluated to be about 45.0 and 19.3 nm, respectively. (b) $I-V$ at room temperature and (c) $R-T$ of dedoped, as-synthesized, and doped polyaniline thin-film devices. (d) SEM image of a polyaniline nanofiber nanodevice (S04). (e) $I-V$ curves of a polyaniline nanodevice under electron-beam exposure at room temperature. (f) Room-temperature resistance of the polyaniline nanodevice as a function of electron-beam exposure time.

energy is simply estimated to be 2 eV by using $U = e^2/4\pi\varepsilon_0\varepsilon_r a$, where e, ε_0, and $\varepsilon_r \cong 2$ are electron charge, vacuum permittivity, and relative permittivity of polyaniline, respectively. After being doped by an acid, the polaron bands form in a protonated chain to demonstrate metallic properties.[13,30] The electrical properties of most of the polyaniline bulk, however, reveal semiconducting rather than metallic manners in the temperature dependence of resistivity.[31] In previous reports,[12,17] the model of conducting grains (Figure 1b) in nanofibers has been proposed for either partially or fully protonated polyaniline. The model of partially protonated polyaniline can readily be considered as protonated regimes, constituting conducting grains and separated by unprotonated polyaniline. On the other hand, as for the model of the fully protonated polyaniline, the amorphous polyaniline, nonstoichiometry or contacts between nanofibers are regarded as insulators separating the conducting grains. The Coulomb (charging) energy E_C between a pair of identical grains of diameter d and the intergrain distance s can be estimated, from the equation[18]

$$E_C = 2Ua/(d(1 + d/2s)) \qquad (1)$$

to be in the range of a hundred millielectronvolts, which is merely 1/10 of the Coulomb energy of electrons sitting at nearest-neighbor benzenes. Figure 1c and its inset present schematically the nanofibrillar nature of polyaniline and the conducting grains in a single nanofiber. In order to exclude the internanotubular contact effects, the conduction mechanism on a mesoscopic scale shall be investigated in a single polyaniline nanofiber. Moreover, instead of using fully protonated polyaniline, we implement

partially protonated polyaniline for studies of the conduction mechanism.

Figure 2a shows a typical scanning electron microscope (SEM) image of as-synthesized polyaniline, revealing a nanofibrillar feature. A statistical distribution of the nanofiber diameters, which were estimated from SEM images, is given in the inset of Figure 2a. After fitting to a Gaussian function, the average diameter with standard deviation was evaluated to be 45.0 ± 19.3 nm. This large standard deviation indicates a wide distribution of the nanofiber diameters and a difficulty in controlling nanofiber morphology. We followed the procedure used in ref 12 to determine the ratio of protonation for a batch of polyaniline samples, thus we could pick up a partially protonated polyaniline sample for the conduction mechanism investigation. Using this partially protonated sample, we can simplify our exploration and ignore the complicated effects of amorphous polyaniline and nonstoichiometry. Electrical characterization of thin-film devices, fabricated using different protonation ratios of polyaniline samples ($NH_3 \cdot H_2O$-dedoped, as-synthesized, and HCl-doped polyaniline), is displayed in Figure 2b,c. The current–voltage ($I-V$) curves of all polyaniline thin-film devices reveal a linear dependence. Evidently, the current increases with HCl protonation, whereas it decreases with $NH_3 \cdot H_2O$ deprotonation. These thin-film devices of dedoped, as-synthesized, and doped polyaniline have room-temperature resistances of 18.80, 1.75, and 0.24 MΩ, specifying a resistance variation of 2 orders of magnitude. This variation is relatively small while it seems to be compatible with data in the previous report.[12] It was learned that the room-temperature resistance cannot be straightforwardly used to determine the protonation ratio. The electron transport behaviors (resistance R as a function of

temperature T) were in turn measured (Figure 2c) and analyzed according to the CELT model[14]

$$R = R_0\exp((T_0/T)^{1/p}) \qquad (2)$$

where $p = 2$, R_0 and T_0 are parameters. It is apparent that all of the three thin-film devices reveal a characteristic $R-T$ behavior in agreement with eq 2. Moreover, the parameter T_0 was evaluated to be about 1.9×10^4, 8.7×10^3, and 3.3×10^3 K for thin-film devices of dedoped, as-synthesized, and doped polyaniline. Comparing the T_0 value with the data in the inset of Figure 2 in ref 12, we determined the protonation ratio of our as-synthesized polyaniline to be about 57%. The as-synthesized sample is then selected as the partially protonated polyaniline and applied to the investigation of the conduction mechanism.

To study electrical properties of a single polyaniline nanofiber, we implemented a nano experimental approach: a standard electron-beam lithography was used to fabricate a pair of electrodes with a nanogap, followed by the dielectrophoresis technique to push the nanofiber into the nanogap. A typical SEM image of the nanofiber devices is displayed in Figure 2d. It is noted that the polyaniline nanofiber is attached on top of the pair of Ti/Au electrodes. Once the nanofiber device was fabricated, it was loaded into an SEM for electron-beam radiation on the contact areas. The step-by-step electron-beam radiation was conducted and followed up with an $I-V$ characterization on the nanofiber device. The data after each electron-beam radiation are presented in Figure 2e. Using the electron-beam radiation, the nonlinear $I-V$ curve of the nanofiber device will gradually change to a straight line, implying a formation of Ohmic contacts and a negligence of contact resistance. The room-temperature resistance as a function of electron-beam exposure time is shown in Figure 2f. The resistance of the nanofiber device decreased up to 3 or 4 orders of magnitudes after electron-beam radiation for 1 h. We found that the electron-beam radiation is particularly useful for the configuration of the nanofiber sitting on top of the electrode. As for the contrary case of the nanofiber buried beneath the electrodes, the effect of electron-beam radiation is reduced owing to a thermal conduction through the metal electrodes. All of the nanofiber devices of our as-synthesized polyaniline were subjected to electron-beam radiation for at least 1 h.

In Figure 3a, we demonstrate $R-T$ behaviors of thin-film devices (L01 and L02) and nanofiber devices (S01–S06) of our as-synthesized polyaniline. The dimensional and fitting parameters of nanofiber devices are listed in Table 1. To rationalize the use of eq 2 for data analysis, we took a nonlinear least-squares fitting with three unspecified parameters of p, R_0, and T_0. The solid curves in Figure 3a represent the best fitting to our data, and the evaluated exponent parameter p
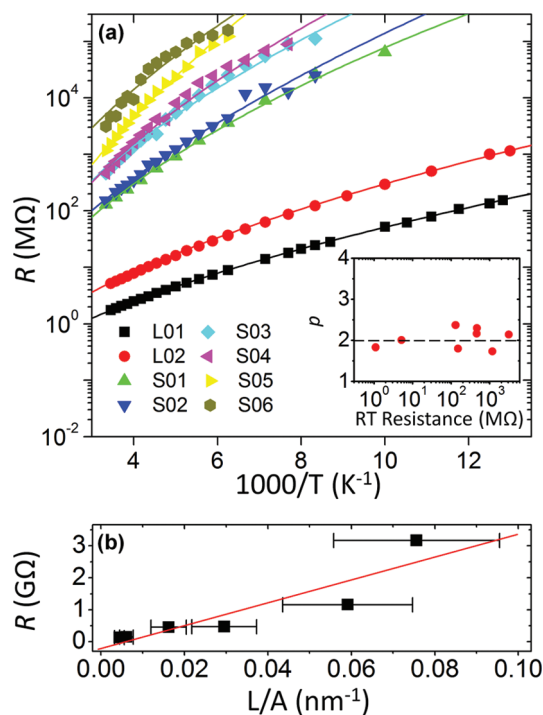
Figure 3. (a) Resistance as a function of inverse temperature for two-probe polyaniline thin-film devices (L01 and L02) and nanodevices (S01–S06). The solid curved lines represent the best fit to data in accordance with the model of charging energy limited tunneling. The cutoff on top of the y-axis is the impedance limitation (100 GΩ) of our measurement system. The inset shows exponent parameters, p, as a function of room-temperature resistance for thin-film and nanoscale devices. The average and standard deviations of the exponent parameter p are 2.08 and 0.28, respectively. (b) Room-temperature resistance as a function of L/A for all polyaniline nanodevices. The solid line is a linear least-squares fitting.

TABLE 1. Room-Temperature (RT) Resistances and Dimensional and Fitting Parameters of As-Synthesized Polyaniline Nanodevices

	RT resistance (GΩ)	T_0 (K)	p	L (nm)	A (nm²)	L/A (nm⁻¹)
S01	0.13	3.1×10^4	2.37	100	22500	0.00044
S02	0.15	4.1×10^4	1.80	142	23130	0.00061
S03	0.45	3.5×10^4	2.16	135	8325	0.01621
S04	0.47	5.1×10^4	2.30	133	4500	0.02955
S05	1.16	3.9×10^4	1.73	266	4500	0.05911
S06	3.12	5.5×10^4	2.14	592	7830	0.0756

values are summarized in the inset. We calculated the average value of p to be 2.08 ± 0.28. This result corroborates our data analysis by using eq 2 with $p = 2$. In addition to the exponent parameter p, we evaluated the average value (4.2×10^4 K) of the T_0 parameter for our nanofiber devices. The T_0 value of the nanofiber devices is higher than that of thin-film devices ($T_0 \cong 8.7 \times 10^3$ K). Moreover, we noticed a large variation of room-temperature resistance, up to 3 orders of magnitude, for our nanofiber devices. We conjecture that the variation of resistance shall come from the dimensions of the nanofibers sitting in the

nanogap. The room-temperature resistance is therefore drawn in Figure 3b as a function of the length L and the cross-sectional area A of the polyaniline nanofibers. The room-temperature resistance R is almost linearly dependent on L/A, suggesting an agreement with the Ohm's law of $R = \rho L/A$, where ρ is the resistivity. The linear least-squares fitting in Figure 3b was conducted to derive a room-temperature resistivity of the as-synthesized polyaniline to be about 10^3 $\Omega \cdot cm$. This value is about 4 orders of magnitude larger than the resistivity ($\sim$0.1 $\Omega \cdot cm$) of fully doped polyaniline, as reported previously.[12]

In addition to the CELT model, there are two other theoretical models, the ES hopping conduction and 1D Mott's VRH, sharing the same mathematical formula of eq 2 with $p = 2$. We examine first the sufficient conditions required to apply the ES hopping conduction to electron transport in a single nanofiber. It was remarked in the literature that the ES hopping conduction can only be observed at temperatures lower than the critical temperature $T_C = e^4 \xi g_0/k_B(4\pi\varepsilon_r\varepsilon_0)^{2,32}$ where e, ξ, g_0, k_B, ε_r, and ε_0 are electron charge, localization length, density of states at Fermi level, Boltzmann constant, relative permittivity, and permittivity of vacuum, respectively. Above the critical temperature, the Coulomb interaction between two localized electron states can be neglected and the Mott's VRH is valid. The localization length ξ can be evaluated using the parameter T_0 and the relation $\xi = 2.8e^2/4\pi\varepsilon_r\varepsilon_0k_BT_0$.[32] In our nanofiber devices, the parameter T_0 is 4.2×10^4 K and the localization length ξ is about 0.6 nm. Taking $\varepsilon_r = 2$ and $g_0 \cong 10^{19}$ eV^{-1} cm^{-3} [33] into account, the critical temperature T_C is estimated to be about 35 K. This critical temperature is definitely lower than the experimental temperature range, implicating that the ES hopping conduction is inadequately adopted to describe electron transport in polyaniline nanofibers. We therefore exclude the possibility of considering the ES hopping model as a conduction mechanism in polyaniline nanofibers.

The next step is to check that whether 1D Mott's VRH or the CELT model is more suitable to describe electron transport in the polyaniline nanofiber. Both of the models suggest the same temperature behavior (eq 2 with $p = 2$) of resistance in the regime of low electric field, but different field dependences of resistance in high electric fields. In the high-field regime, the differential resistance as a function of electric field E is expressed as[14,20]

$$R = R_T \exp((E_0/E)^{1/q}) \quad (3)$$

where E_0 and q are constant parameters and R_T is a temperature-dependent parameter. It is argued that the exponent parameter q values are 1 and 2 for the CELT model and 1D Mott's VRH, respectively. In the high-field regime, the resistance measurement is more difficult since a high voltage up to 100 V is required for
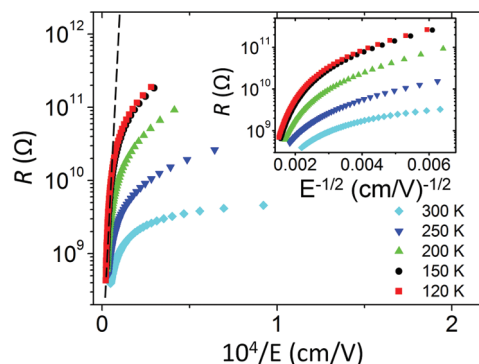
Figure 4. Differential resistance R (dV/dI) *versus* inverse electric field (1/E) of S06 nanofiber device at various temperatures. The dashed line indicates a high-field approached curve. The data in the form of dV/dI *versus* $E^{-1/2}$ are also presented in the inset for comparison.

thin-film devices to create a strong field. Using the nano experimental approach (the nanofiber devices), we only need to apply a low voltage of 10 V to create such a high electric field. Figure 4 displays the differential resistance on a logarithm scale as a function of inverse electric field (E^{-1}) at various temperatures. Obviously, the resistance tends to collapse into a line (the dashed line in Figure 4) in the high-field regime. The data at lower temperature reveal a higher tendency to approach a linear dependence. From fitting the data in high-field regime (close to the dash line) to eq 3, we evaluated the E_0 parameter to be 1.5×10^6 V/cm. This value is 20 times larger than that evaluated in a previous report.[12] Furthermore, the T_0 value of the nanofiber devices is about 4 or 5 times larger than that of the thin-film devices. These high E_0 and T_0 values could be beneficially coming from our nano approach investigation. On the other hand, the resistance on a logarithm scale as a function of $E^{-1/2}$ is plotted in the inset of Figure 4, but no trend of a single line approach has ever been observed. Consequently, we believe that the data can be better described by the CELT model.

According to Sheng's CELT model,[14] we can use the two parameters, T_0 and E_0, to discuss elaborately the conduction mechanism in a single polyaniline nanofiber. The basic assumption of the model is that the intergrain distance s multiplied by the charging energy E_C of the grain is a constant. The charging energy of the grain E_C is inversely proportional to the grain diameter d, so the assumption leads to a constant ratio of s/d. The average of $s + d$ values can be estimated from the expression $s + d = (k_BT_0)/(4eE_0)$.[14] Using the T_0 of 5.5×10^4 K and E_0 of 1.5×10^6 V/cm for the S06 nanofiber device, we calculated the $s + d$ value to be about 7.7 nm. This $s + d$ value, which is shorter than the diameter of the nanofiber ($\sim$45 nm), is quite reasonable. Additionally, the ratio of s/d can be determined from the T_0 parameter and the relation of $T_0 = 8U/k_B(d/s + (d/s)^2/2)$.[34] This relation is a generalized derivation of the CELT model when finding the most probable value
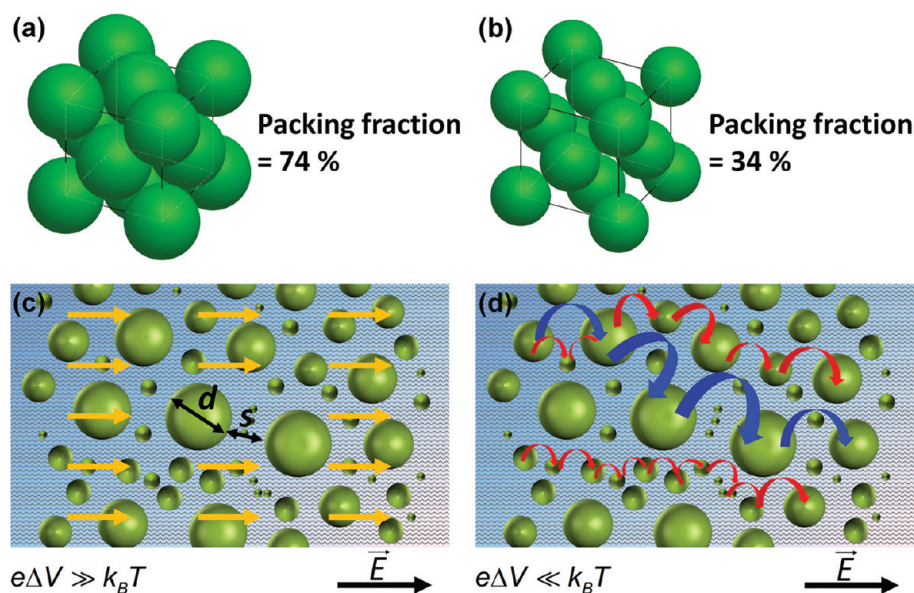
Figure 5. (a) Face-centered cubic structure of conducting grains. (b) Face-centered cubic structure of conducting grains with a nonzero intergrain distance. Schematic diagrams of the conducting model in the polyaniline nanofiber in (c) high- and (d) low-field regime. The solid zig-zagged lines represent polyaniline polymer chains. The deep green sphere implies conducting grains of protonated polyaniline (emeraldine salt), which is surrounded by insulating regions of unprotonated polyaniline (emeraldine base form). The average diameter, d, and the separation distance, s, of the metallic regions are marked on the graph. The arrows in orange indicate the conducting paths resulting from a high electric field. The red and blue curved arrows hint at the conducting paths of the thermally activated hopping transport in a low electric field at high and low temperatures, respectively.

of the intergrain distance s.[18] The s/d ratio is evaluated to be about 0.6 for the S06 nanofiber device. Thus, the average of intergrain distance s and the grain diameter d are about 2.8 and 4.9 nm, respectively. The charging energy of the conducting grains can then be estimated to be ∼78 meV from eq 1. This high charging energy, which is higher than thermal energy at room temperature (25 meV), ascertains that the CELT model can be applied to the temperature range of our experiment.

To understand more about the CELT model, we assume that the partially protonated polyaniline consists of protonated regimes (conducting grains) and unprotonated, intergrain regimes with a grain diameter of 4.9 nm and an intergrain distance of 2.8 nm. We use a hard sphere model arranged in a face-centered cubic (fcc) structure (Figure 5a). Taking the conducting grains as hard spheres contacted with each other, we obtain a packing fraction of 74%. In this case, the system shall be metallic since the conducting grains are connected through intergrain contacts. Now if the grain diameter and the average intergrain distance are scaled to 4.9 and 2.8 nm, the packing fraction is decreased to 34%. The long and the short intergrain distances, used in Figure 5b, are 4.1 and 1.5 nm, respectively. That packing fraction is smaller than the protonation ratio of 57% estimated from the T_0 parameter of the thin-film device of as-synthesized polyaniline. The difference could result from a fluctuation of protonation ratio in the nanofiber, regarded as a number of resistors connected in series. The measured resistance is dominated by the resistor with the largest

resistance and the lowest protonation ratio. The correspondence between the CELT model and the real system of polyaniline nanofibers still needs further theoretical work. Schemes of electron transport in high- and low-electric-field regimes are given in Figure 5c,d, respectively. In high electric field, the electric-field-created potential energy between grains is much higher than the thermal energy, so the field-induced tunneling dominates in the generation of charge carriers between grains. The rate of tunneling is reduced exponentially with the intergrain distance,[14] and additionally, an increase of electric potential energy gives an equivalent effect as shortening the intergrain distance as well as increasing the tunneling rate (charge carriers). The charge transport can take path along different diameters of conducting grains (see Figure 5c). On the other hand, the thermally activated charge carriers dominate in the low-field regime. At a low temperature, the charge carriers transport through a hopping path to consume a low charging energy, requiring a hopping through large conducting grains (see the blue curved arrow in Figure 5d). At higher temperatures, more and more hopping channels are established between smaller grains, and the charge carriers can hop through either the large or the small grains (the red curved arrows in Figure 5d).

CONCLUSIONS

We synthesized partially protonated polyaniline nanofibers and determined the protonation ratio to be

57% by analyzing the temperature-dependent resistance of thin-film devices. Techniques of electron-beam lithography and dielectrophoresis are implemented to fabricate nanofiber devices of the as-synthesized polyaniline. Through data analysis, we argued that the conduction mechanism is best described by the CELT model, rather than the ES hopping or the 1D Mott's VRH model. Using the CELT model to analyze temperature- and electric-field-dependent resistances of nanofiber devices, we estimated the values of T_0 and E_0 parameters to be larger than those calculated from data of thin-film devices. The T_0 and E_0 parameters are applied to determine the conducting grain diameter ($\sim$4.9 nm) and the intergrain distance ($\sim$2.8 nm) in a single nanofiber. According to the CELT model, electron transport in a single polyaniline nanofiber is expressed schematically in detail. In a high electric field, the electric-field-induced tunneling dominates charge transport. In a low electric field, the thermal-energy-activated tunneling is in competition with the Coulomb charging energy of the conducting grains. Thus the carriers take the hopping path through large conducting grains at low temperatures, and more and more hopping paths connecting small grains are established with increasing temperature. The *true* conduction mechanism on a *mesoscopic* scale is explored and elucidated in a single polyaniline nanofiber through the nano experimental approach.

METHODS

Synthesis. Polyaniline nanofibers were synthesized by using a rapidly mixed reaction.[35] A description of the synthesis method is given as follows. A solution of ammonium persulfate (0.183 g, 0.8 mmol, >99%, Sigma-Aldrich Ltd.) dissolved in 10 mL of 1 M HCl was carefully poured in a solution of aniline (0.298 g, 3.2 mmol, >99%, Sigma-Aldrich Ltd.) dissolved in 10 mL of 1 M HCl. The mixed solution was stirred immediately at room temperature. The polymerization began, and the mixed solution had turned a deep green color. This solution was stirred continuously for 24 h. To store polymer solution, 0.5 mL of this solution was fetched and diluted with distilled water of 10 mL. Polyaniline nanofibers were stocked in the water solution.

Microscopy. Samples were prepared by dropping the polyaniline solution on Si wafers, having a dimension of 7 × 7 mm², and they were dried before microscopy measurements. The samples were loaded in a high vacuum chamber of a field-emission scanning electron microscope (JEOL JSM-7000F). Dimensions and morphology of polyaniline nanofibers were all recorded using FE-SEM.

Thin-Film Devices. By means of a standard photolithography technique, micrometer-scale Ti/Au ($\sim$10/60 nm in thickness) electrodes were deposited on Si wafers capped with a 400 nm thick SiO₂ layer to prevent any possible current leakage through the substrate. The separation distance between two nearest-neighbor electrodes was about 40 μm. The as-synthesized polyaniline solution was either protonated or deprotonated by washing with 0.25 M HCl or 0.2 M NH₃·H₂O solution, respectively. Thin-film devices were prepared by dropping these polyaniline solutions on the photolithographically prepatterned Si wafer and dried for hours at room temperature in air.

Nanofiber Devices. In connection with prepatterned micrometer-scale electrodes on Si wafers, a standard electron-beam lithography technique was used to deposit two submicrometer Ti/Au ($\sim$20/100 nm thickness) current leads and to leave a gap of 100$-$600 nm in width. The resistance between the two current leads and across the empty gap was determined to be much higher than 1 TΩ in a bias voltage of $\pm$10 V, implying a negligible, low leakage current at room temperature. This high empty-gap resistance guarantees a real measurement of electrical properties if the current, flowing through the as-deposited, crossing-gap material, is much higher than the leakage current. Here the dielectrophoresis technique was applied to position polyaniline nanofibers into the gap. To fabricate nanofiber devices, several drops of polyaniline solutions were put on the empty-gap device and an alternative current (AC) voltage of 1 MHz sinusoidal wave was imposed between two submicrometer current leads for 3 min. Thus polyaniline nanofibers were attracted and positioned into the gap. It is noted that, depending on the width of the gap, the AC driving voltage was varied

between 3 and 6 V. Moreover, a capacitor of 10 μF was seriously connected during the dielectrophoresis process in prevention of any direct-current-induced electrochemical reactions. After the dielectrophoresis process, excess polyaniline solution was gently blown off the nanofiber device by using nitrogen gas. In order to improve electrical contacts between polyaniline nanofibers and submicrometer leads, the contact pads of the nanofiber devices were exposed to the electron beam of FE-SEM with a dose of 3 × 10⁴ C/m²·s for at least 1 h.

Electrical Property. Either thin-film or nanofiber two-probe devices were loaded in a cryostat (variable temperature insert cryostat, CRYO Industries of America Inc.) in helium gas (99.99%) at 760 Torr for acquisition of temperature-dependent electrical behaviors from 300 to 80 K. The current$-$voltage measurements were carried out by using either Keithley K-6430 or a homemade system. The homemade electrometer demonstrates a current and voltage resolution of 10 pA and 1 mV, respectively. The impedance limitation of our system, including the cryostat and the electrometer, is about 100 GΩ. The resistance was estimated around the zero bias voltage from the current$-$voltage curves, and its standard deviation was evaluated to be less than 0.1%.

REFERENCES AND NOTES

1. Genies, E. M.; Boyle, A.; Lapkowski, M.; Tsintavis, C. Polyaninline—A Historical Survey. *Synth. Met.* **1990**, *36*, 139–182.
2. Huang, W. S.; Humphrey, B. D.; MacDiarmid, A. G. Polyaniline, a Novel Conducting Polymer. *J. Chem. Soc., Faraday Trans. 1* **1986**, *82*, 2385–2400.
3. Jozefowicz, M. E.; Laversanne, R.; Javadi, H. H. S.; Epstein, A. J.; Pouget, J. P.; Tang, X.; MacDiarmid, A. G. Multiple Lattice Phases and Polaron-Lattice-Spinless-Defect Competition in Polyaniline. *Phys. Rev. B* **1989**, *39*, 12958–12961.
4. Chiang, C. K.; Fincher, C. R.; Park, Y. W.; Heeger, A. J.; Shirakawa, H.; Louis, E. J.; Gau, S. C.; MacDiarmid, A. G. Electrical Conductivity in Doped Polyacetylene. *Phys. Rev. Lett.* **1977**, *39*, 1098–1101.
5. Surwade, S. P.; Manohar, N.; Manohar, S. K. Origin of Bulk Nanoscale Morphology in Conducting Polymers. *Macromolecules* **2009**, *42*, 1792–1795.
6. Huang, J.; Virji, S.; Weiller, B. H.; Kaner, R. B. Nanostructured Polyaniline Sensors. *Chem.—Eur. J.* **2004**, *10*, 1314–1319.

7. Baker, C. O.; Shedd, B.; Innis, P. C.; Whitten, P. G.; Spinks, G. M.; Wallace, G. G.; Kaner, R. B. Monolithic Actuators from Flash-Welded Polyaniline Nanofibers. *Adv. Mater.* **2008,** *20*, 155–158.

8. Kim, B. K.; Kim, Y. H.; Won, K.; Chang, H.; Choi, Y.; Kong, K. J.; Rhyu, B. W.; Kim, J. J.; Lee, J. O. Electrical Properties of Polyaniline Nanofiber Synthesized with Biocatalyst. *Nanotechnology* **2005,** *16*, 1177–1181.

9. Tseng, R. J.; Huang, J; Ouyang, J.; Kanner, R. B.; Yang, Y. Polyaniline Nanofiber/Gold Nanoparticle Nonvolatile Memory. *Nano Lett.* **2005,** *5*, 1077–1080.

10. Bélanger, D.; Ren, X.; Davey, J.; Uribe, F.; Gottesfeld, S. Characterization and Long-Term Performance of Polyaniline-Based Electrochemical Capacitors. *J. Electrochem. Soc.* **2000,** *147*, 2923–2929.

11. Tran, H. D; Wang, Y.; D'Arcy, J. M.; Kanner, R. B. Toward an Understanding of the Formation of Conducting Polymer Nanofibers. *ACS Nano* **2009,** *2*, 1841–1848.

12. Zuo, F.; Angelopoulos, M.; MacDiarmid, A. G. Transport Studies of Protonated Emeraldine Polymer: A Granular Polymeric Metal System. *Phys. Rev. B* **1987,** *36*, 3475–3478.

13. Stafstrom, S.; Bredas, J. L.; Epstein, A. J.; Woo, H. S.; Tanner, D. B.; Huang, W. S.; MacDiarmid, A. G. Polaron Lattice in Highly Conducting Polyaniline: Theoretical and Optical Studies. *Phys. Rev. Lett.* **1987,** *59*, 1464–1467.

14. Sheng, P.; Abeles, B.; Arie, Y. Hopping Conductivity in Granular Metals. *Phys. Rev. Lett.* **1973,** *31*, 44–47.

15. Wang, Z. H.; Li, C.; Scherr, E. M.; MacDiarmid, A. G.; Epstein, A. J. Three Dimensionality of "Metallic" States in Conducting Polymer: Polyaniline. *Phys. Rev. Lett.* **1991,** *66*, 1745–1748.

16. Li, Q.; Cruz, L.; Philips, P. Granular-Rod Model for Electronic Conduction in Polyaniline. *Phys. Rev. B* **1993,** *47*, 1840–1845.

17. Pelster, R.; Nimtz, G.; Wessling, B. Fully Protonated Polyaniline: Hopping Transport on a Mesoscopic Scale. *Phys. Rev. B* **1994,** *49*, 12718–12723.

18. Zuppiroli, L.; Bussac, M. N.; Paschen, S.; Chauvet, O.; Forro, L. Hopping in Disordered Conducting Polymers. *Phys. Rev. B* **1994,** *50*, 5196–5203.

19. Li, W.; Wan, M. Porous Polyaniline Films with High Conductivity. *Synth. Met.* **1998,** *92*, 121–126.

20. Joo, J.; Long, S. M.; Pouget, J. P.; Oh, E. J.; MacDiarmid, A. G.; Epstein, A. J. Charge Transport of the Mesoscopic Metallic State in Partially Crystalline Polyanilines. *Phys. Rev. B* **1998,** *57*, 9567–9580.

21. Ghosh, M.; Barman, A.; De, S. K.; Chatterjee, S. Crossover from Mott to Efros-Schklovskii Variable-Range-Hopping Conductivity in Conducting Polaniline. *Synth. Met.* **1998,** *97*, 23–29.

22. Planès, J.; Wolter, A.; Cheguettine, Y.; Proń, A.; Genoud, F.; Nechtschein, M. Transport Properties of Polyaniline-Cellulose-Acetate Blends. *Phys. Rev. B* **1998,** *58*, 7774–7785.

23. Chaudhuri, D.; Kumar, A.; Nirmala, R.; Sarma, D. D.; García-Hernández, M.; Sharath, L. S.; Ganesan, V. Transport and Magnetic Properties of Conducting Polyaniline Doped with BX_3 (X = F, Cl, and Br). *Phys. Rev. B* **2006,** *73*, 075205.

24. Tzamalis, G.; Zaidi, N. A.; Monkman, A. P. Applicability of the Localization-Interaction Model to Magnetoconductivity Studies of Polyaniline Films at the Metal−Insulator Boundary. *Phys. Rev. B* **2003,** *68*, 245106.

25. Li, D.; Wang, Y.; Xia, Y. Electrospining of Polymeric and Ceramic Nanofibers as Uniaxially Alligned Arrays. *Nano Lett.* **2003,** *3*, 1167–1171.

26. Kameoka, J.; Orth, R.; Yang, Y.; Czaplewski, D.; Mathers, R.; Coates, G. W.; Craighead, H. G. A Scanning Tip Electrospinning Source for Deposition of Oriented Nanofibres. *Nanotechnology* **2003,** *14*, 1124–1129.

27. Pinto, N. J.; Johnson, A. T., Jr.; MacDiarmid, A. G.; Mueller, C. H.; Theofylaktos, N.; Robinson, D. C.; Miranda, F. A. Electrospun Polyaniline/Polyethylene Oxide Nanofiber Field-Effect Transistor. *Appl. Phys. Lett.* **2003,** *83*, 4244–4246.

28. Long, Y.; Chen, Z.; Wang, N.; Ma, Y.; Zhang, Z.; Zhang, L.; Wan, M. Electrical Conductivity of a Single Conducting Polyaniline Nanotube. *Appl. Phys. Lett.* **2003,** *83*, 1863–1865.

29. Aleshin, A. N. Polymer Nanofibers and Nanotubes: Charge Transport and Device Applications. *Adv. Mater.* **2006,** *18*, 17–27.

30. Varela-Álvarez, A.; Sordo, J. A. A Suitable Model for Emeraldine Salt. *J. Chem. Phys.* **2008,** *128*, 174706.

31. Lee, K.; Cho, S.; Park, S. H.; Heeger, A. J.; Lee, C. W.; Lee, S. H. Metallic Transport in Polyanilline. *Nature* **2006,** *441*, 65–68.

32. Efros, A. L.; Shklovskii, B. I. Coulomb Gap and Low Temperature Conductivity of Disordered Systems. *J. Phys. C: Solid State Phys.* **1975,** *8*, L49–L51.

33. Ghosh, M.; Barman, A.; De, S. K.; Chatterjee, S. Transport Properties of HCl Doped Polyaniline and Polyaniline-Methylcellulose Dispersion. *J. Appl. Phys.* **1998,** *84*, 806–811.

34. Wolter, A.; Rannou, P.; Travers, J. P. Model for Aging in HCl-Protonated Polyaniline: Structure, Conductivity, and Composition Studies. *Phys. Rev. B* **1998,** *58*, 7637–7647.

35. Huang, J.; Kaner, R. B. Nanofiber Formation in the Chemical Polymerization of Aniline: A Mechanistic Study. *Angew. Chem., Int. Ed.* **2004,** *116*, 5941–5945.